Chemotaxis of *Escherichia coli* to Norepinephrine (NE) Requires Conversion of NE to 3,4-Dihydroxymandelic Acid

Sasikiran Pasupuleti,[a] Nitesh Sule,[a] William B. Cohn,[b] Duncan S. MacKenzie,[b] Arul Jayaraman,[a] Michael D. Manson[b]

Department of Chemical Engineering[a] and Department of Biology,[b] Texas A&M University, College Station, Texas, USA

Norepinephrine (NE), the primary neurotransmitter of the sympathetic nervous system, has been reported to be a chemoattractant for enterohemorrhagic *Escherichia coli* (EHEC). Here we show that nonpathogenic *E. coli* K-12 grown in the presence of 2 μM NE is also attracted to NE. Growth with NE induces transcription of genes encoding the tyramine oxidase, TynA, and the aromatic aldehyde dehydrogenase, FeaB, whose respective activities can, in principle, convert NE to 3,4-dihydroxymandelic acid (DHMA). Our results indicate that the apparent attractant response to NE is in fact chemotaxis to DHMA, which was found to be a strong attractant for *E. coli*. Only strains of *E. coli* K-12 that produce TynA and FeaB exhibited an attractant response to NE. We demonstrate that DHMA is sensed by the serine chemoreceptor Tsr and that the chemotaxis response requires an intact serine-binding site. The threshold concentration for detection is ≤5 nM DHMA, and the response is inhibited at DHMA concentrations above 50 μM. Cells producing a heterodimeric Tsr receptor containing only one functional serine-binding site still respond like the wild type to low concentrations of DHMA, but their response persists at higher concentrations. We propose that chemotaxis to DHMA generated from NE by bacteria that have already colonized the intestinal epithelium may recruit *E. coli* and other enteric bacteria that possess a Tsr-like receptor to preferred sites of infection.

The human gastrointestinal (GI) tract harbors an assortment of bacteria, most of which are harmless or helpful commensals. However, infection of the GI tract by pathogenic bacteria can have devastating consequences. It has been suggested that norepinephrine (NE), the predominant neurotransmitter of the enteric sympathetic nervous system, promotes growth and virulence of enteric bacteria (1) through signaling via adrenergic receptors located either on intestinal epithelial cells (2) or in the bacteria themselves (3, 4). In particular, the bacterial quorum sensor kinase QseC has been implicated in the NE-induced expression of genes whose products are involved in adherence, motility, and pathogenesis (4, 5). However, the concentrations of NE required for effective induction of virulence genes, 50 μM in one recent study (6), are higher than those that are expected to occur in the intestinal lumen (7, 8). Thus, for NE to activate expression of virulence factors, bacteria would have to navigate to regions of the intestinal epithelium that have locally high concentrations of NE. An obvious candidate for directing such migration is chemotaxis.

Chemotaxis in *Escherichia coli* is well understood at the molecular level. However, the compounds that have been reported as chemoattractants (9) are primarily nutrients: serine and related amino acids, sensed by the chemoreceptor Tsr; aspartate and maltose, sensed by Tar; ribose and galactose, sensed by Trg; and dipeptides and pyrimidines, sensed by Tap. NE has been reported to be an interdomain signaling molecule (5, 10, 11). NE serves as an inducer of virulence and motility genes in enterohemorrhagic *E. coli* (EHEC) and in *Salmonella enterica* (6, 10). The primary signaling pathway for induction of virulence appears to go through the membrane-bound quorum-sensing kinase QseC and its associated response regulator, QseB (12). The relationship between stress and microbial infection suggests that increased catecholamine concentrations in the intestine promote bacterial growth (13) and colonization (14). However, the effects of NE in enhancing virulence require higher concentrations than those that are predicted to exist in the gut, and in some cases, they appear to be independent of QseC and instead related to the ability of NE to

serve as an iron chelator (15). However, both α- and β-adrenergic receptor antagonists inhibit the responses of enteric bacteria to catecholamines, and receptors other than QseC, including QseE, BasS, and CpxA, have been reported to contribute to the bacterial response to adrenergic signals (5). The current study was undertaken to determine the mechanisms underlying chemotaxis to NE as a first step toward investigating whether chemotaxis contributes to the virulence of enteric bacteria.

MATERIALS AND METHODS

Bacterial strains and solutions. Strain CV1 is equivalent to strain RP437 (16) but was renamed to conform to the nomenclature of other strains used in this study. It was used as the wild-type *E. coli* strain for chemotaxis. All relevant strains and plasmids are listed in Table 1. Liquid cultures were grown in tryptone broth (TB; 10 g/liter tryptone and 8 g/liter NaCl). Selection for kanamycin resistance was done on Luria-Bertani agar containing 1.2% Difco Bacto agar and 50 μg/ml kanamycin. TB semisolid agar contained 0.35% Difco Bacto agar. H1 minimal-glycerol TLHMB$_1$ agar contained 1.2% Difco Bacto agar and was supplemented with 0.5% glycerol, 20 μg/ml (each) threonine, leucine, histidine, and methionine, and 1 μg/ml thiamine. Chemotaxis buffer (CB) consisted of physiological buffered saline with 10 mM potassium phosphate, pH 7.0, containing 0.1 mM EDTA, 0.01 mM L-methionine, and 10 mM DL-lactate. Expression of Tsr from plasmids pCA24N-*tsr* and pRR53-*tsr*$_{R69E}$ was induced with 100 μM isopropyl-β-D-thiogalactopyranoside (IPTG). This concentration of inducer gave optimal serine chemotaxis in tryptone semisolid agar when wild-type Tsr was expressed from pCA24N-*tsr* in the Δ*tsr* strain CV5.

TABLE 1 Strains and plasmids used in this study

Strain or plasmid	Relevant genotype or other characteristics	Antibiotic resistance[a]	Source or reference
E. coli strains			
CV1	Wild type for chemotaxis; equivalent to RP437 *thr-1*(Am) *leuB6 his-4 metF159*(Am) *rpsL136* [*thi-1 ara-14 lacY1 mtl-1 xyl-5 eda tonA31 tsx-78*]	Str	[16]
CV5	CV1 Δ*tsr thr*⁺	Str	[50]
CV12	CV1 (*tar-tap*)Δ*5201 trg*::Tn*10 eda*⁺	Str, Tet	[50]
CV16	CV1 Δ*tsr thr*⁺ (*tar-tap*)Δ*5201 trg*::Tn*10 eda*⁺	Str, Tet	[50]
BW25113 Δ*tynA*	BW25113 *tynA*ΩKan	Kan	[17]
BW25113 Δ*feaB*	BW25113 *feaB*ΩKan	Kan	[17]
BW25113 Δ*qseC*	BW25113 *qseC*ΩKan	Kan	[17]
SP101	CV1 Δ*tynA*	Str, Kan	This study
SP102	CV1 Δ*feaB*	Str, Kan	This study
SP103	CV1 Δ*qseC*	Str, Kan	This study
UU2641	RP437 *serB*::*kan-ccdB*	Str, Kan	J. S. Parkinson, personal communication
UU2375	RP437 *tsr*-R69E (*tar-tap*)Δ*5201* (*aer*)Δ*1 ygjG*::Gm (*trg*)Δ*4543*	Str	Parkinson, personal communication
UU2376	RP437 *tsr*-R69E (*tar-tap*)Δ*5201* (*aer*)Δ*1 ygjG*::Gm (*trg*)Δ*4543*	Str	Parkinson, personal communication
TAMU100	CV1 *serB*::*kan-ccdB*		This study
TAMU101	CV1 *tsr*-R69E		This study
TAMU102	CV1 *tsr*-T156K		This study
TAMU104	TAMU101/pRR53-*tsr*$_{R69E}$		This study
TG1	*supE thi-1* Δ(*lac-proAB*) Δ(*mcrB-hsdSM*)5 (r$_K$⁻ m$_K$⁻) F′ [*traD36 proAB*⁺ *lacI*�q *lacZ*ΔM15]		Stratagene
Plasmids			
pCM18	GFP expression vector	Erm	[51]
pDS-Red Express	RFP expression vector	Amp	Clontech
pRR53-*tsr*$_{R69E}$	Expresses Tsr-R69E under the control of IPTG	Amp	[36]

[a] Abbreviations: Str, streptomycin; Tet, tetracycline; Kan, kanamycin; Erm, erythromycin; Cm, chloramphenicol; Amp, ampicillin.

Reagents. 3,4-Dihydroxymandelic acid (DHMA; 98% pure) was obtained from Sigma-Aldrich, and norepinephrine (>99.5% purity) was obtained from Calbiochem.

Generation of mutants. The *tynA*, *feaB*, and *qseC kan*-insertion knockout mutations in strains SP101 to -103 were introduced into strain CV1 by phage P1$_{vir}$ transduction from the respective mutants in the Keio collection (17), with selection for resistance to 50 μg/ml kanamycin. The insertions were confirmed by Southern blotting. Chromosomal *tsr* point mutations were introduced into strain CV1 in two steps. First, a *serB-kan* insertion from strain UU2641 was introduced into strain CV1 by P1$_{vir}$ transduction, with selection for resistance to 50 μg/ml kanamycin on Luria broth (LB) agar, to generate strain TAMU100. The *tsr* mutations were then introduced into strain TAMU100 by P1$_{vir}$ transduction with lysates prepared on strains UU2375 and UU2376, which contain chromosomal *tsr* alleles encoding Tsr-R69E and Tsr-T156K, respectively, to generate strains TAMU101 and TMAU102. Selection for Ser⁺ transductants was accomplished by plating on minimal-glycerol TLHMB₁ agar, and the presence of the *tsr* mutations was screened by testing transductants on TB semisolid agar and picking isolates that did not form the outer (serine) chemotaxis ring. Glycerol was used as the carbon source in minimal medium because glucose adventitiously induces transcription of the *ccdB* (control of cell death) gene from the *rhaB* promoter in the *kan* insertion that allows counterselection for loss of the insertion in the presence of rhamnose (18). CcdB is a potent gyrase inhibitor (19) that is the toxin of an addiction system of the F plasmid of *E. coli* (20).

Fabrication of microflow devices. Microflow devices were fabricated as previously described (21). Briefly, device designs were drawn in Auto-CAD and used to create a high-resolution (>3,000 dots per in. [dpi]) photolithography mask with a laser printer (Advanced Reproductions, North Andover, MA). Standard photolithography techniques using an SU-8 2050 photoresist (Microchem Corp., MA) generated imprints of the microflow devices on silicon wafers. The silicon wafer templates were used as negative molds to generate the chemotaxis devices in poly(dimethyl) siloxane (PDMS), using standard soft-lithography protocols (21). Chamber dimensions were measured using a profilometer. Devices were fabricated by bonding the patterned PDMS slab to clean glass slides, using oxygen-plasma bonding in a plasma etcher (100 mtorr, 100 W, 40 s) to create optically transparent devices. Access ports were punched into the PDMS by use of a blunt 19-gauge needle.

Microflow assay. The microflow assay for chemotaxis (21) measures the chemotaxis response of bacteria fluorescently labeled by green fluorescent protein (GFP) expression. When the cells enter the observation chamber, they encounter a stable concentration gradient of chemoeffector established across the width of the microfluidic chamber. The microflow chemotaxis device consists of two modules: a concentration gradient generator and a chemotaxis observation chamber. The gradient generator comprises a network of microfluidic channels that uses diffusive mixing from five inputs to generate nonlinear, approximately exponential concentration gradients across the width of the observation chamber. The length of the network is 18.5 mm. The width of each inlet entering the observation chamber is 500 μm. The observation module is a chamber (20 μm × 1,050 μm × 2 cm) connected to the gradient generator module. A secondary inlet (50 μm) is used to introduce bacteria into the observation module at the midpoint of the concentration gradient. The bacteria and the concentration gradients are introduced into the device through silicon tubing. The device infused with dyes of different colors is shown in Fig. S1 in the supplemental material.

The assay was performed as described previously (21). A mixture of GFP-expressing, motile test cells and red fluorescent protein (RFP)-containing, dead TG1 cells was gently resuspended in CB containing the che-

moeffector at the concentration expected at the midpoint of the observation chamber and incubated for 20 min. All steps were conducted at room temperature. The flow rate in the microfluidic device was controlled using a PicoPlus programmable pump (Harvard Apparatus, Holliston, MA). The assembled device was positioned on the stage of a Leica TCS SP5 resonant-scanner confocal microscope. Multiple 500-μl gas-tight glass syringes (Hamilton, Reno, NV), containing either CB or CB with chemoeffector, were carefully connected to the inlets of the gradient generator module to avoid introducing air bubbles into the device. The bacterial mixture was introduced into the chemotaxis chamber through the bacterial inlet port, using a 50-μl gas-tight glass syringe. The syringes connected to the gradient generator and the bacterial inlet were operated at the same flow rate, using different pumps. The total flow rate in the observation module (from the five gradient inlets and one bacterial inlet) was maintained at 2.1 μl/min. Green and red fluorescent images were acquired for 20 min. For each experiment, 100 images for each fluorophore were collected 7 mm from the inlet at 2.5-s intervals. The 2.5-s imaging interval was chosen based on our calculation that free-floating bacteria moving at a flow rate of 2.1 μl/min take an average of 2.5 to 3 s to traverse 1,000 μm, the imaging field of view (21). Therefore, bacteria in the middle of the flow were exposed to the gradient for an average of 18 to 21 s prior to imaging. Cells spending more time in contact with the floor or ceiling of the chamber move more slowly (22).

Quantification of chemotaxis in the microflow assay with image analysis. The migration and distribution of bacteria in each image were quantified using a Matlab (Mathworks, Natick, MA) image analysis subroutine developed in-house, as described previously (21). Briefly, the analysis consisted of the following steps: (i) removal of background pixels in the image, based on pixel size and intensities; (ii) determination of the center of the image (i.e., where bacteria enter the observation chamber), using dead cells (red fluorescence) as a reference; (iii) location of green cells (i.e., live bacteria expressing GFP) in the images relative to the center, determined by calculating the centroid; and (iv) quantification of the number of live cells in 16-μm-wide intervals. These steps were repeated for each image, and the total counts of cells in 100 images were summed for analysis. The images shown in Fig. 7 and in Fig. S2 in the supplemental material show the 100 images combined into a single composite image.

The migration profile was used to calculate the chemotaxis migration coefficient (CMC), which weights the migration of cells by the distance they move from the center of the observation chamber, as previously described (23). For example, a cell that moves to the farthest high-concentration position at the right (interval 64) receives a weighting factor of +1, and a cell that moves to the farthest low-concentration position at the left (interval 1) is given a weighting factor of −1. Green cells in the middle of the chamber (intervals 31 to 34) were excluded from the analysis on the grounds that they could be nonmotile or poorly motile cells. The motility migration coefficient (MMC) was determined in the same way, except that the weighting factor was positive in both directions. Examples of assays used to calculate CMC and MMC values are shown in Fig. S2 in the supplemental material.

The CMC value represents the magnitude of the chemotaxis response to the steep exponential gradients that are generated with 10-fold increases in the attractant concentration in each of the five inlet ports, from left to right. The cells were preincubated for 10 min with the same concentration of attractant present in the middle (third) inlet, which is the concentration they experience when entering the chamber. The MMC value represents the extent of the smooth-swimming response of cells in CB that are introduced into a chamber with a uniform concentration of attractant. The cells do not adapt to the attractant until they spread across the chamber. If they adapt before reaching the point along the channel at which their distribution is imaged, their movement will be random run-and-tumble behavior that will not significantly affect the final distribution across the chamber.

Preparation of motile bacteria for chemotaxis assays. Bacteria were prepared for chemotaxis assays as described by Mao et al. (23). Cultures of GFP-expressing bacteria, grown overnight at 32°C in TB containing 150 μg/ml erythromycin, were inoculated into 25 ml of the same medium lacking erythromycin to a turbidity at 600 nm of ~0.05. Cultures were grown with swirling in 125-ml Erlenmeyer flasks at 32°C to mid-exponential phase (turbidity at 600 nm of ~0.5), with the addition of 100 μM IPTG for induction of Tsr expression from the pRR53-*tsr* and pCA24N-*tsr* plasmids. A 3-ml aliquot of cells was centrifuged at 400 × *g* for 5 min at room temperature and gently resuspended in 2 ml of CB. TG1 cells expressing RFP were killed by exposure to 1 mM kanamycin for 1 h (complete killing was verified by a lack of growth on LB agar plates), thoroughly washed with CB, and mixed with GFP-expressing motile cells at approximately equal densities. The microflow chemotaxis assay was performed within 20 min after resuspension of the bacteria in CB, which contained attractants at the concentration expected at the midpoint of the observation chamber, e.g., 500 nM in a 0- to 50-μM exponential gradient. In some experiments, bacteria were prepared as described above but primed by addition of 2 μM NE to the TB growth medium 1 h before harvesting. Cells introduced into uniform concentrations of attractants were resuspended in nonsupplemented CB, except as noted.

RNA isolation and qRT-PCR. Bacteria were grown using the protocol described above for the microflow assay, with or without priming. After 60 min of exposure to NE, cells were collected by centrifugation and stored at −80°C prior to RNA extraction. RNA was extracted using a Nucleospin RNA II kit (Clontech, CA) according to the protocol recommended by the manufacturer. Cells grown without NE were used as negative controls. Total RNA was isolated from the cell pellets, and RNA quality was assessed spectrophotometrically. Quantitative reverse transcription-PCR (qRT-PCR) was performed using an iScript one-step RT-PCR kit with SYBR green (Bio-Rad Laboratories, CA) on a MyiQ single-color real-time PCR detection system (Bio-Rad Laboratories). The threshold cycles calculated by the MyiQ optical system software (Bio-Rad Laboratories) were used to determine the relative changes between samples. The experiments were run in triplicate in 25-μl reaction mixtures, and 50 ng of total RNA was used for each reaction mixture, with a final forward and reverse primer concentration of 0.15 μM (each). After amplification, template specificity was ensured through melting curve analysis. The *rrsG* (rRNA G) transcript was used as the housekeeping RNA for normalizing the data.

Determination of the number of molecules of DHMA in the periplasm. The mean volume of an *E. coli* cell grown in a moderately rich medium, such as TB, has been estimated to be around 4 fl (24), and the volume of the periplasm has been estimated to be 20 to 40% of the total cell volume (25). Thus, 1×10^{-15} liter is a reasonable estimate for the average periplasmic volume. At 5 nM (5×10^{-9} mol/liter), a concentration of DHMA that still generates an attractant response, there are thus about 5×10^{-24} mol of DHMA in the periplasm, assuming equilibration with the external medium. Multiplying by Avogadro's number (6×10^{23} molecules/mol), this yields about 3 molecules of DHMA in the periplasmic space of a single cell.

RESULTS

An *E. coli* K-12 strain shows chemotaxis toward NE. To examine NE chemotaxis, we used the K-12 strain RP437 (16), a standard for studies of *E. coli* chemotaxis. Strain RP437 is henceforth called CV1 to conform to the nomenclature used for the chemoreceptor mutant strains used in this study.

We employed a microflow device manufactured in-house (21) to monitor chemotaxis to NE. This assay offers several advantages for studying the response to biological signals. First, the microliter volumes involved minimize the amount of a chemical that must be used per assay. Second, the migration of bacteria can be observed in stable gradients of almost any desired profile. These gradients are established in a mixing device and are oriented perpendicular to the direction of flow. Third, because the microflow
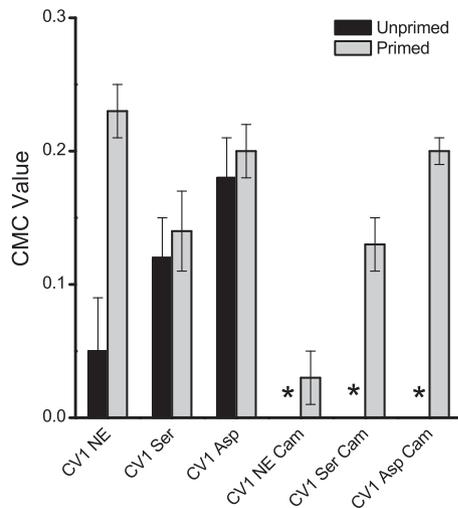
FIG 1 CMC values for cells in exponential gradients of 1 to 500 μM NE and 1 to 200 μM serine and aspartate. Error bars represent the standard deviations of the means for results from triplicate experiments. Primed cells were grown in the presence of 2 μM NE for 1 h before harvesting. Abbreviations: CB, chemotaxis buffer; NE, norepinephrine; Asp, aspartate; Ser, serine; Cam, chloramphenicol. *, not assayed.

chamber is only 1 mm wide, the gradients formed can be very steep. Finally, the time for the bulk flow to reach the site of imaging is ~20 s, so the short-term responses of cells can be recorded.

Cells harvested from TB did not respond to NE in the microflow assay, in contrast to the results of earlier reports with a microplug assay (10). However, in the microplug assay, cells are exposed to NE for 30 min or longer. We therefore tested whether prior exposure to NE primes cells to respond. Cells grown in TB

supplemented with 2 μM NE for 1 h before harvesting showed a robust response to NE (Fig. 1) that was equivalent to the response observed with similar gradients of serine (Fig. 1; see Fig. S2 in the supplemental material). The effects of preexposure to NE were eliminated when 12.5 μg/ml chloramphenicol was added at the same time as NE, suggesting that protein synthesis is required for the effect (Fig. 1). Chemotaxis to serine and aspartate, sensed as attractants by the Tsr and Tar chemoreceptors, respectively, was unaffected by chloramphenicol. These results suggest that preincubation with NE induces the synthesis of proteins that are required for NE to be sensed as an attractant.

Chemotaxis toward NE requires induction of bacterial enzymes. One pathway for NE metabolism in mammals involves deamination to form 3,4-dihydroxyphenyl-glycol-aldehyde (DOPEGAL) followed by oxidation to form 3,4-dihydroxymandelic acid (DHMA) (26). These steps in *E. coli* can potentially be carried out by two enzymes: a periplasmic tyramine oxidase, TynA (27), and a cytoplasmic aromatic aldehyde dehydrogenase, FeaB (27). qRT-PCR analysis showed that *tynA* transcription increased 4.5-fold and *feaB* transcription increased 3.5-fold after 1 h of incubation with 2 μM NE (Fig. 2B). The SP101 and SP102 mutants, which lack TynA and FeaB, respectively, failed to respond to NE in the microflow assay (Fig. 3).

The quorum-sensing kinase QseC has been implicated in NE-induced expression of virulence and motility genes in pathogenic *E. coli* and *S. enterica* (4, 5). Induction of *tynA* and *feaB* transcription by exposure to NE was abolished in the Δ*qseC* mutant SP103 (Fig. 2B), which also showed a large decrease in NE chemotaxis (Fig. 3). These results suggest that NE sensed by QseC induces *tynA* and *feaB* transcription, and hence production of DOPEGAL and DHMA.

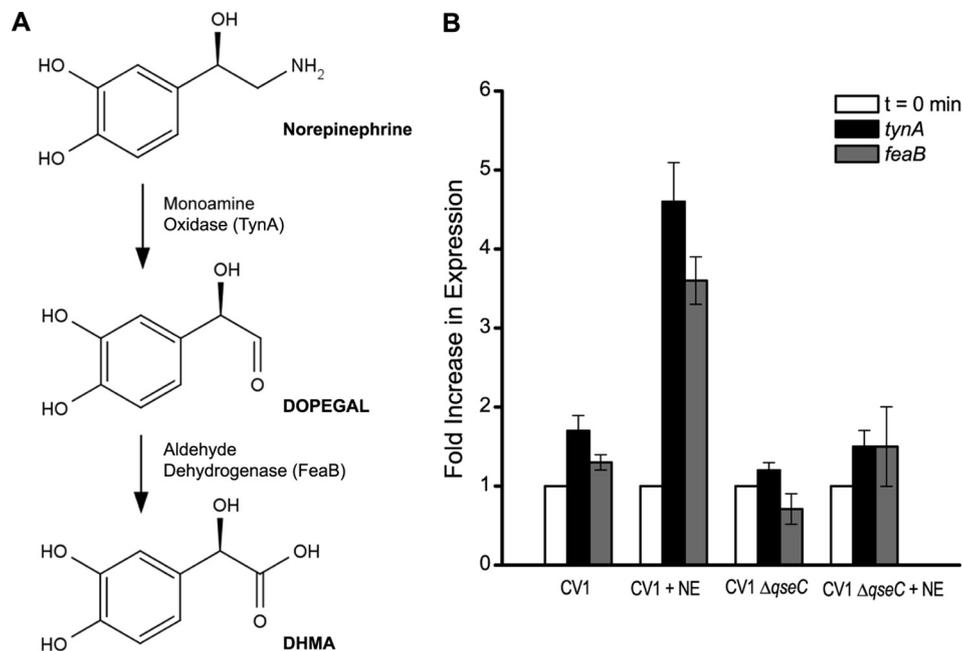**DHMA is a potent attractant for *E. coli*.** DOPEGAL is not

FIG 2 Bacterial genes encode enzymes that can produce DHMA from NE. (A) The chemical pathway shown is present in the human GI tract, and *E. coli* potentially has a similar capability via TynA and FeaB, as indicated. (B) Induction of *tynA* and *feaB* transcription by preincubation with 2 μM NE in wild-type and Δ*qseC* cells. The levels of transcript were measured by qRT-PCR 60 min after addition of 2 μM NE to the culture for 1 h. Controls were grown over this period in the absence of NE. The results are normalized to the level of the *rrsG* transcript. The error bars represent the standard deviations of the means.
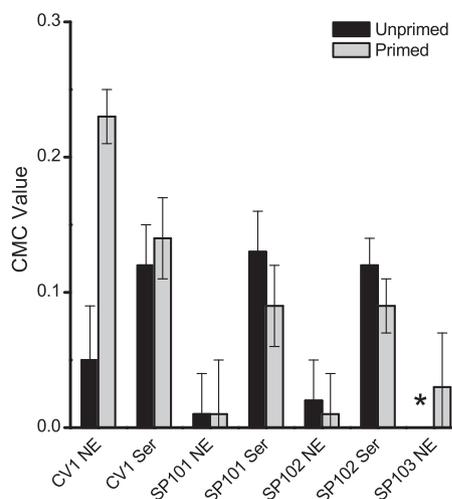
FIG 3 NE chemotaxis in mutants defective in NE metabolism. CMC values are shown for exponential gradients of 0 to 500 µM NE and 0 to 200 µM serine. Strains: CV1, wild type; SP101, Δ*tynA* strain; SP102, Δ*feaB* strain; SP103, Δ*qseC* strain. Error bars represent the standard deviations of the means for results from triplicate experiments. Primed cells were grown in the presence of 2 µM NE for 1 h before harvesting. *, not assayed.

commercially available, but DHMA proved to be a very strong attractant for strain CV1 (Fig. 4). Representative images of the microflow assays with DHMA are shown in Fig. S2 in the supplemental material. The response to DHMA was strongest in an exponential gradient of 0 to 50 µM. The CMC value was 0.12 in a gradient of 0 to 5 µM, 0.22 in a gradient of 0 to 50 µM, 0.09 in a gradient of 0 to 500 µM, and 0.06 in a gradient of 0 to 5,000 µM (Fig. 4). The simplest explanation for the decreased response at higher concentrations of DHMA is that the receptor became sat-
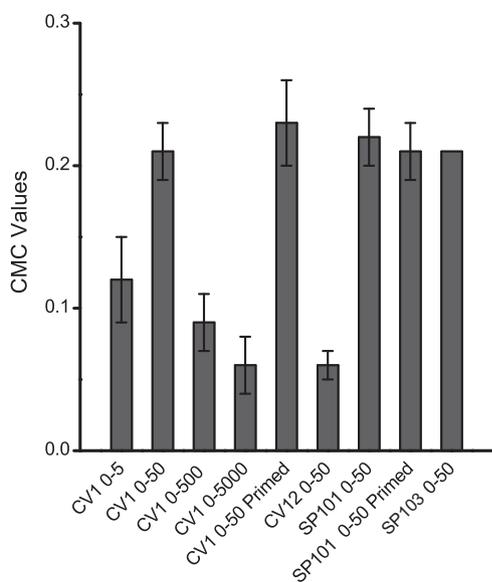

FIG 4 CMC values for cells in exponential DHMA gradients. The gradients ranged from 0 to the indicated value, in µM. Strains: CV1, wild type; CV12, Δ*tar-tap* Δ*trg* strain; SP101, Δ*tynA* strain; SP103, Δ*qseC* strain. Error bars represent the standard deviations of the means for results from triplicate experiments. Primed cells were grown in the presence of 2 µM NE for 1 h before harvesting.
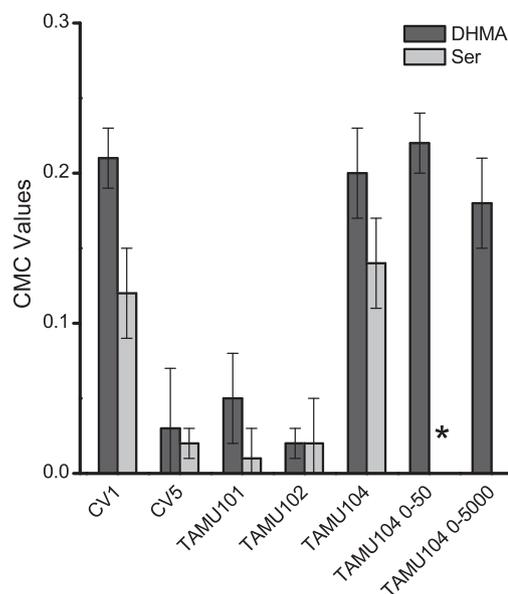

FIG 5 DHMA chemotaxis in *tsr* mutant strains. CMC values are shown for exponential gradients of 0 to 50 µM DHMA and 0 to 200 µM serine. Strains: CV1, wild type; CV5, Δ*tsr* strain; TAMU101, *tsr*-R69E strain; TAMU102, *tsr*-T156K strain; TAMU104, strain expressing a chromosomal *tsr*-T156K gene and a plasmid-borne *tsr*-R69E gene at approximately the same levels. CMC values are also given for TAMU104 in gradients of 0 to 500 µM and 0 to 5,000 µM DHMA for comparison with the CMC values in those gradients for strain CV1 shown in Fig. 4. Error bars represent the standard deviations of the means for results from triplicate experiments. Primed cells were grown in the presence of 2 mM NE for 1 h before harvesting. *, not assayed.

urated. Strain CV12, which contains only Tsr and Aer, gave a much weaker response to DHMA. This difference may be due to altered ligand sensitivity in strains that contain only one type of high-abundance chemoreceptor (28, 29). Note that this response is highly unlikely to be an aerotactic response through Aer, as strains lacking a functional Tsr receptor did not show any response in the microfluidic assay. Moreover, the device is not designed to either generate or maintain gaseous gradients within the flow chamber, as has been reported by Adler et al. (30).

Chemotaxis to DHMA requires the Tsr chemoreceptor and its intact serine-binding site. CV5 cells that lack Tsr did not respond to serine or DHMA, although their response to aspartate was the same as that of CV1 cells (Fig. 5). We then tested whether the serine-binding site of Tsr is required for sensing DHMA. The T156K and R69E amino acid replacements in Tsr disrupt the majority and minority halves, respectively, of the serine-binding site (31). Strains TAMU101 and TAMU102, which encode Tsr-R69E and Tsr-T156K, respectively, at the chromosomal *tsr* locus, also failed to respond to serine or DHMA in the microflow assay (Fig. 5). This analysis suggests that the DHMA- and serine-binding sites in Tsr overlap.

Heterodimeric Tsr with one functional ligand-binding site mediates responses to DHMA. Tsr contains two rotationally symmetric serine-binding sites that exhibit strong negative cooperativity (32) (Fig. 6A). We therefore tested the possibility that binding of DHMA at the second site inhibits the attractant signal produced by binding at the first site. The Tsr-T156K and Tsr-R69E mutant subunits were produced at approximately equal levels in strain TAMU104 (see Materials and Methods). In this strain, the T156K
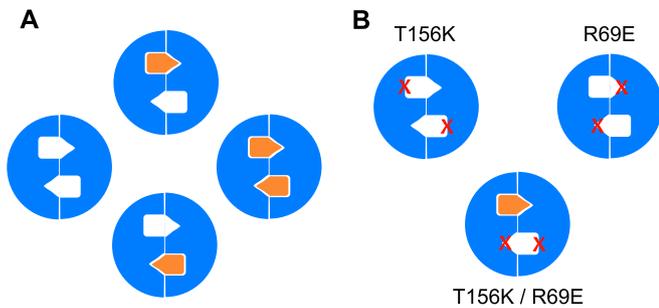
FIG 6 Complementation of mutations that disrupt the majority and minority half-binding sites for serine in the Tsr dimer. (A) Periplasmic domain of the wild-type Tsr homodimer. Squares indicate the majority site, and triangles indicate the minority site. The receptor monomers are shown in blue, and the ligands are shown in orange, with the square end representing the α-amino and α-carboxyl groups of the amino acid ligand and the pointed end representing the R group. Ligands can bind with equal affinities to either of the rotationally symmetric binding sites. Both sites can be occupied, but binding to the second typically occurs with strong negative cooperativity. (B) The residue substitutions introduced by mutations, indicated by the red X's, are T156K for the majority site and R69E for the minority site. Neither mutant homodimer is capable of binding ligand. If the two mutant receptors are coexpressed at equal levels, half of the Tsr dimers will be heterodimers (T156K/R69E) that retain one intact ligand-binding site.

protein is expressed from the chromosomal *tsr* locus, and the R69E protein is expressed from a plasmid-carried *tsr* gene under the control of an IPTG-inducible promoter. After induction with 100 μM IPTG, this strain produces approximately the same amount of Tsr as the chromosomal gene. Under these conditions, half of the Tsr molecules should be heterodimers with one intact ligand-binding site and one doubly defective site (Fig. 6B). A similar approach has been used to show that Tar (33, 34) and Tsr (35, 36) heterodimers of this type still mediate attractant responses to their respective ligands. In contrast to CV1 cells, TAMU104 cells exposed to 100 μM IPTG responded robustly to DHMA in gradients of 0 to 50 μM up to 0 to 5,000 μM (Fig. 5). Thus, when Tsr has

only one functional ligand-binding site, it mediates good chemotaxis responses at higher concentrations of DHMA.

In a second assay, cells resuspended in CB in the absence of DHMA were introduced into a microflow chamber containing various uniform concentrations of DHMA in CB. In this assay, a smooth-swimming response is indicated by enhanced spreading of cells in both directions from the midpoint, where they enter the channel. This spreading is quantified in a term we call the motility migration coefficient (MMC) (see Materials and Methods). The difference in the responses used to determine the CMC and MMC values is illustrated in Fig. 7A, and the full spectrum of responses to uniform concentrations of DHMA and serine is presented in Fig. S2 in the supplemental material. A more complete discussion of the behaviors quantified in the CMC and MMC assays is given in Materials and Methods, under the heading "Quantification of chemotaxis in the microflow assay with image analysis."

Wild-type CV1 cells had an MMC value of 0.16 in CB. In comparison, exclusively smooth-swimming CV16 cells, which lack all four canonical chemoreceptors, had an MMC value of 0.40 in CB. The increased spreading of smooth-swimming cells probably occurs because they rapidly reach the floor or ceiling of the 20-μm-tall chamber and move laterally in the channel without being caught up in the bulk flow, which would quickly wash them through the chamber. Thus, they have more time to spread across the width of the chamber.

As shown in Fig. 7B, CV1 and TAMU104 cells already showed increased MMC values at 5 nM (0.0005 μM) DHMA, whereas TAMU101 (Tsr$_{R69E}$) and TAMU102 (Tsr$_{T156K}$) cells first showed increased MMC values at 500 nM (0.5 μM) and 5 μM DHMA, respectively. Thus, the two point mutations in *tsr* do not make the cells totally unresponsive to DHMA, but they decrease the response sufficiently to prevent detectably higher CMC values in exponential DHMA gradients in our microflow assay. CV1 cells introduced into the chamber after being exposed to DHMA for 20 min at the same concentration as that they encountered in the chamber did not show MMC values above 0.16 at any DHMA
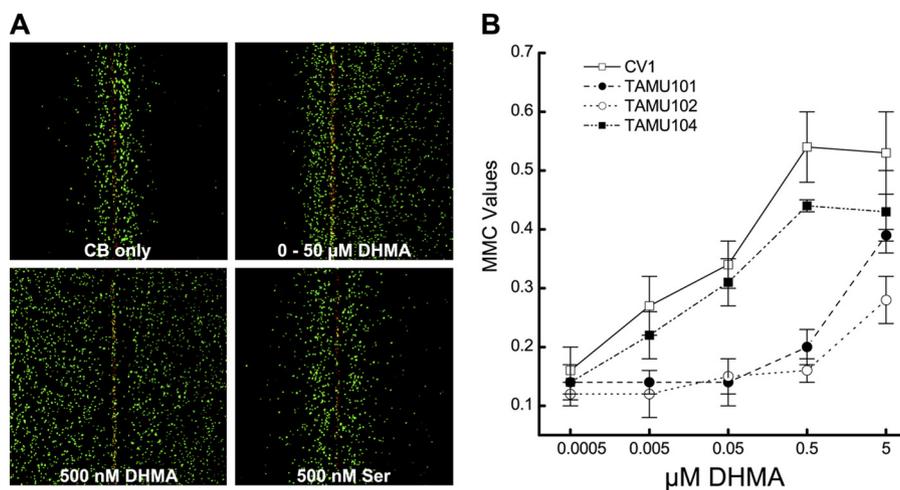

FIG 7 (A) Representative images of the microflow assay illustrating both CMC and MMC assays. (Top left) CB only; (top right) exponential gradient of 0 to 50 μM DHMA; (bottom left) uniform concentration of 500 nM DHMA; (bottom right) uniform concentration of 500 nM serine. (B) MMC values for different *tsr* mutants in exponential gradients of DHMA from 0 to the indicated concentration, in μM. Strains: CV1, wild type; TAMU101, *tsr*-R69E strain; TAMU102, *tsr*-T156K strain; TAMU104, strain with chromosomal *tsr*-T156K and plasmid-borne, salicylate-inducible *tsr*-R69E. Error bars represent the standard deviations of the means for results from triplicate experiments.
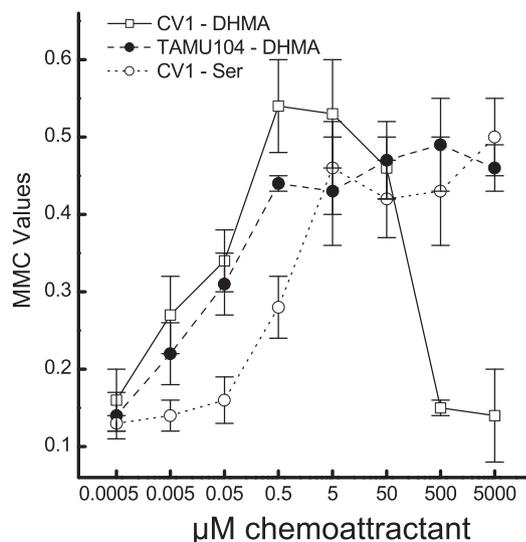
FIG 8 MMC values for different *tsr* mutants in exponential gradients from 0 to the indicated concentration of DHMA or serine, in µM. Strains: CV1, wild type; TAMU104, strain with chromosomal *tsr*-T156K and plasmid-borne, salicylate-inducible *tsr*-R69E. The DHMA data for CV1 are an extension of those shown in Fig. 7B. Error bars represent the standard deviations of the means for results from triplicate experiments.

concentration, so the cells did adapt to the presence of DHMA, as they do to serine.

CV1 cells first showed an increase in MMC value at 500 nM serine, indicating that Tsr senses DHMA about 100 times more sensitively than it senses serine (Fig. 8). The MMC values for serine plateaued at 5 µM and remained between 0.40 and 0.45 up to 5 mM. The MMC values plateaued at 0.5 to 0.55 with 0.5 and 5 µM DHMA but then dropped significantly at 500 µM DHMA. The MMC values at 500 µM and 5 mM DHMA were the same as those of the buffer control. In contrast, TAMU104 cells expressing heterodimeric Tsr with only one ligand-binding site responded with increased MMC values at DHMA concentrations of up to 5 mM, although they reached their plateau value of 0.40 to 0.5 at a 0.5 µM concentration of DHMA, as was the case with CV1 cells. This result is consistent with the idea that DHMA interacts with the second Tsr ligand-binding site to cancel out the attractant signal evoked by binding at the first site. We saw no obvious increase in tumbling at high concentrations of DHMA, which should be reflected in lower MMC values. Therefore, binding to the second site does not generate an obvious repellent response. Binding at the second site must occur with a lower affinity, as expected because of the negative cooperativity that exists between the two sites (32, 37).

DISCUSSION

This study made the following discoveries. (i) The RP437 K-12 strain of *E. coli* exhibits chemotaxis to NE. This highly motile, nonpathogenic strain possesses all of the chemoreceptors found in EHEC (38) and shares the high-abundance chemoreceptors Tar and Tsr with *S. enterica*. (ii) Chemotaxis to NE requires induction of the periplasmic tyramine oxidase, TynA, and the aromatic aldehyde dehydrogenase, FeaB, through a signaling pathway that requires the quorum-sensing histidine protein kinase QseC. Thus, the observed chemotaxis response to NE is indirect. (iii) DHMA, a

metabolite of NE that can potentially be made by the combined activities of TynA and FeaB, is a potent chemoattractant for *E. coli* K-12, with effective concentrations of ≤5 nM, suggesting that chemotaxis to NE is actually chemotaxis to DHMA. (iv) DHMA is sensed by the serine chemoreceptor Tsr. (v) Mutant variants of Tsr defective in the majority (Tsr-T156K) or minority (Tsr-R69E) half of the cross-dimer serine-binding site are defective in DHMA chemotaxis. (vi) A heterodimeric receptor that consists of one subunit of Tsr-T156K and one subunit of Tsr-R69E and has only one functional serine-binding site mediates good chemotaxis to DHMA. (vii) Cells expressing wild-type Tsr show a decreased response to DHMA at concentrations above 50 µM, whereas cells expressing the Tsr-156K/Tsr-R69E heterodimer do not show a decreased chemotaxis response at high concentrations of DHMA. Although these results make the basic mechanism of chemotaxis to NE and DHMA clear, they leave several questions unanswered.

How can cells respond to such low concentrations of DHMA? Assuming equilibration between the concentrations of unbound small molecules in the environment and the periplasm, at an external DHMA concentration of 5 nM there should be about 3 molecules of free periplasmic DHMA (see Materials and Methods). Diffusion of small molecules trapped within the periplasmic space is very rapid, so localization of the chemoreceptors at subpolar patches (39) should not be limiting for the kinetics of detection of DHMA. If Tsr binds DHMA very tightly, then the number of Tsr receptors occupied by DHMA at 5 nM DHMA may be considerably larger than 3. In any case, the response to DHMA is exquisitely sensitive.

The binding of one additional attractant molecule per second is adequate to cause a measurable increase in counterclockwise flagellar bias (40, 41). Rates of change in bound DHMA should certainly occur in cells moving laterally in the steep gradients present in the observation chamber of our microflow device. The sensitivity of the response is enhanced by the high level of amplification seen within the receptor patch (the activity of ~35 CheA kinases inhibited per molecule of attractant bound [28]) and by the high positive cooperativity (Hill coefficient of ~11) in adjusting the rotational bias of the flagellar motor to changes in intracellular CheY-phosphate (42).

Why is the microflow assay ideal for studying chemotaxis to biological signals? The observation chamber in the microflow assay is only 20 µm high. Thus, chemotaxis in the microflow assay is essentially a two-dimensional excursion. This geometry may provide a good simulation of the spatial context in which chemotaxis occurs in the intestine. The physiologically relevant response to NE or its metabolites in the intestine could be largely a surface phenomenon that occurs when the cells swim within or under the mucosal layer, which is only a few hundred micrometers thick and lies in close proximity to the intestinal epithelium. The gradients in the microflow assay can be made very steep, a condition that may also reflect the situation *in vivo*. With conventional assays for chemotaxis, it is unlikely that we could have observed a response that peaks at 5 to 50 µM DHMA and then disappears at higher concentrations. We anticipate that the microflow assay will be suitable for screening bacterial chemotaxis to a wide range of biological signaling molecules in a spatial and temporal context similar to that in which chemotaxis probably occurs in the host intestine.

Why do cells respond only to low concentrations of DHMA? Unlike the typical situation, in which responses plateau at high

concentrations of attractant, the smooth-swimming response to DHMA disappears at higher concentrations (Fig. 8). This effect is not seen if the second of the two ligand-binding sites of the Tsr homodimer is eliminated, as in the R69E/T156K heterodimer (Fig. 6B). One possible explanation is that DHMA binds to the second site with negative cooperativity (32, 37) and, by so doing, cancels out the attractant signal generated by binding to the first site. The mechanism for this phenomenon remains to be elucidated, but *in vivo* it would be expected to cause cells to congregate in regions with intermediate concentrations of DHMA.

Is NE/DHMA chemotaxis an important factor in gut-microbe interactions? The DHMA that bacteria encounter in the GI tract may be generated by the host or by bacterial metabolism. The ability of NE to induce the synthesis of bacterial enzymes that convert NE to DHMA suggests that resident bacteria may play an important role in generating localized DHMA gradients. Because FeaB and the other aldehyde dehydrogenases are presumably confined to the cytoplasm, to respond to NE the DOPEGAL generated by periplasmic TynA would have to be taken up by the cells and converted to DHMA, which would then have to be released back into the periplasm. A similar mechanism is observed for *E. coli* chemotaxis to lactose (43). Lactose must be taken up into the cell by lactose permease (44) and split into glucose and galactose by β-galactosidase (45). One or both of these monosaccharides must then reenter the periplasm and bind to the MglB binding protein (46), which then has to interact with the Trg chemoreceptor (47). However, in the intestine, motile cells probably respond to DHMA gradients generated by bacteria that have already colonized the intestinal epithelium. Thus, sensitivity to low concentrations of DHMA is consistent with the idea that chemotaxis to DHMA has biological significance.

Endogenous DHMA production is normally low in sympathetic neuronal tissues (26), but it may be produced from NE by bacteria that have already colonized NE-rich areas on the intestinal epithelium. Among such sites would be the Peyer's patches near the junction of the jejunum and ileum, which are favored locations for colonization and invasion by enteric bacteria (48). By navigating to loci of NE leakage, cells may encounter the higher concentrations of NE that are required for induction of virulence genes (6). Furthermore, stress increases release of NE by the sympathetic innervation of the gut and heightens the severity of bacterial infection in the GI tract (7), and high levels of NE enhance growth of *E. coli* in serum-based media *in vitro* (13). This effect is also seen as a temporary and reversible increase in fecal coliforms in the mouse intestine in the presence of pharmacologically induced high levels of NE in the mouse (14). The combination of induction of virulence genes by NE and chemotaxis to its metabolite DHMA may work together to heighten the pathogenicity of enteric bacteria that possess a Tsr-like chemoreceptor.

It is intriguing that the serine receptor Tsr, typically reported to be the most abundant of the *E. coli* chemoreceptors (49), also senses two biological signaling molecules, the intradomain quorum-sensing compound AI-2 (50) and the interdomain signaling molecule DHMA. It is exciting to contemplate that microfluidic assays may uncover other secrets about old friends in the chemotaxis signaling pathways of bacteria.

ACKNOWLEDGMENTS

REFERENCES

1. **Freestone PP, Lyte M, Neal CP, Maggs AF, Haigh RD, Williams PH.** 2000. The mammalian neuroendocrine hormone norepinephrine supplies iron for bacterial growth in the presence of transferrin or lactoferrin. J. Bacteriol. **182:**6091–6098. http://dx.doi.org/10.1128/JB.182.21.6091-6098.2000.
2. **Green BT, Brown DR.** 2010. Interactions between bacteria and the gut mucosa. Do enteric neurotransmitters acting on the gut mucosal epithelium influence intestinal colonization or infection?, p 89–110. *In* Lyte ML, Freestone PPE (ed), Microbial endrocrinology: interkingdom signaling in infectious disease and health. Springer, New York, NY.
3. **Moreira CG, Sperandio V.** 2010. The epinephrine/norepinephrine/autoinducer-3 interkingdom signaling system of Escherichia coli O157:H7, p 213–227. *In* Lyte ML, Freestone PPE (ed), Microbial endrocrinology: interkingdom signaling in infectious disease and health. Springer, New York, NY.
4. **Clarke MB, Hughes DT, Zhu C, Boedeker EC, Sperandio V.** 2006. The QseC sensor kinase: a bacterial adrenergic receptor. Proc. Natl. Acad. Sci. U. S. A. **103:**10420–10425. http://dx.doi.org/10.1073/pnas.0604343103.
5. **Karavolos MH, Winzer K, Williams P, Khan CMA.** 2013. Pathogen espionage: multiple bacterial adrenergic sensors eavesdrop on host communication systems. Mol. Microbiol. **87:**455–465. http://dx.doi.org/10.1111/mmi.12110.
6. **Moreira CG, Weinshenker D, Sperandio V.** 2010. QseC mediates Salmonella enterica serovar Typhimurium virulence in vitro and in vivo. Infect. Immun. **78:**914–926. http://dx.doi.org/10.1128/IAI.01038-09.
7. **Lyte M, Vlcahnova L, Brown D.** 2011. Stress at the intestinal surface: catecholamines and mucosa-bacteria interactions. Cell Tissue Res. **343:**23–32. http://dx.doi.org/10.1007/s00441-010-1050-0.
8. **Stevens MP.** 2010. Modulation of the interaction of enteric bacteria with intestinal mucosa by stress-related catecholamines, p 111–134. *In* Lyte ML, Freestone PPE (ed), Microbial endrocrinology: interkingdom signaling in infectious disease and health. Springer, New York, NY.
9. **Hazelbauer GL, Falke JJ, Parkinson JS.** 2008. Bacterial chemoreceptors: high-performance signaling in networked arrays. Trends Biochem. Sci. **33:**9–19. http://dx.doi.org/10.1016/j.tibs.2007.09.014.
10. **Bansal T, Englert D, Lee J, Hegde M, Wood TK, Jayaraman A.** 2007. Differential effects of epinephrine, norepinephrine, and indole on Escherichia coli O157:H7 chemotaxis, colonization, and gene expression. Infect. Immun. **75:**4597–4607. http://dx.doi.org/10.1128/IAI.00630-07.
11. **Roshchina VV.** 2010. Evolutionary considerations of neurotransmitters in microbial, plant, and animal cells, p 17–52. *In* Lyte ML, Freestone PPE (ed), Microbial endrocrinology: interkingdom signaling in infectious disease and health. Springer, New York, NY.
12. **Kostakioti M, Hadjifrangiskou M, Pinkner JS, Hultgren SJ.** 2009. QseC-mediated dephosphorylation of QseB is required for expression of genes associated with virulence in uropathogenic Escherichia coli. Mol. Microbiol. **73:**1020–1031. http://dx.doi.org/10.1111/j.1365-2958.2009.06826.x.
13. **Lyte M, Ernst S.** 1992. Catecholamine induced growth of gram negative bacteria. Life Sci. **50:**203–212. http://dx.doi.org/10.1016/0024-3205(92)90273-R.
14. **Lyte M, Bailey MT.** 1997. Neuroendocrine-bacterial interactions in a neurotoxin-induced model of trauma. J. Surg. Res. **70:**195–201. http://dx.doi.org/10.1006/jsre.1997.5130.
15. **Pullinger GD, Carnell SC, Sharaff FF, van Diemen PM, Dziva F, Morgan E, Lyte M, Freestone PPE, Stevens MP.** 2010. Norepinephrine augments Salmonella enterica-induced enteritis in a manner associated with increased net replication but independent of the putative adrenergic sensor kinases QseC and QseE. Infect. Immun. **78:**372–380. http://dx.doi.org/10.1128/IAI.01203-09.
16. **Parkinson JS, Houts SE.** 1982. Isolation and behavior of Escherichia coli deletion mutants lacking chemotaxis functions. J. Bacteriol. **151:**106–113.
17. **Baba T, Ara T, Hasegawa M, Takai Y, Okumura Y, Baba M, Datsenko KA, Tomita M, Wanner BL, Mori H.** 2006. Construction of Escherichia

coli K-12 in-frame, single-gene knockout mutants: the Keio collection. Mol. Syst. Biol. **2**:2006.0008. http://dx.doi.org/10.1038/msb4100050.

18. **Wang H, Bian X, Xia L, Ding X, Muller R, Zhang Y, Fu J, Stewart AF.** 2014. Improved seamless mutagenesis by recombineering using ccdB for counterselection. Nucleic Acids Res. **42**:e37. http://dx.doi.org/10.1093/nar/gkt1339.

19. **Bernard P, Couturier M.** 1992. Cell killing by the F plasmid CcdB protein involves poisoning of DNA-topoisomerase II complexes. J. Mol. Biol. **226**:735–745. http://dx.doi.org/10.1016/0022-2836(92)90629-X.

20. **Jaffe A, Ogura T, Hiraga S.** 1985. Effects of the ccd function of the F plasmid on bacterial growth. J. Bacteriol. **163**:841–849.

21. **Englert DL, Jayaraman A, Manson MD.** 2009. Microfluidic techniques for the analysis of bacterial chemotaxis. Methods Mol. Biol. **571**:1–23. http://dx.doi.org/10.1007/978-1-60761-198-1_1.

22. **Englert DL, Manson MD, Jayaraman A.** 2009. Flow-based microfluidic device for quantifying bacterial chemotaxis in stable, competing gradients. Appl. Environ. Microbiol. **75**:4557–4564. http://dx.doi.org/10.1128/AEM.02952-08.

23. **Mao H, Cremer PS, Manson MD.** 2003. A sensitive, versatile microfluidic assay for bacterial chemotaxis. Proc. Natl. Acad. Sci. U. S. A. **100**:5449–5454. http://dx.doi.org/10.1073/pnas.0931258100.

24. **Volkmer B, Heinemann M.** 2011. Condition-dependent cell volume and concentration of Escherichia coli to facilitate data conversion for systems biology modeling. PLoS One **6**:e23126. http://dx.doi.org/10.1371/journal.pone.0023126.

25. **Stock JB, Rauch B, Roseman S.** 1977. Periplasmic space in Salmonella typhimurium and Escherichia coli. J. Biol. Chem. **252**:7850–7861.

26. **Eisenhofer G, Kopin IJ, Goldstein DS.** 2004. Catecholamine metabolism: a contemporary view with implications for physiology and medicine. Pharmacol. Rev. **56**:331–349. http://dx.doi.org/10.1124/pr.56.3.1.

27. **Rankin LD, Bodenmiller DM, Partridge JD, Nishino SF, Spain JC, Spiro S.** 2008. Escherichia coli NsrR regulates a pathway for the oxidation of 3-nitrotyramine to 4-hydroxy-3-nitrophenylacetate. J. Bacteriol. **190**:6170–6177. http://dx.doi.org/10.1128/JB.00508-08.

28. **Sourjik V, Berg HC.** 2004. Functional interactions between receptors in bacterial chemotaxis. Nature **428**:437–441. http://dx.doi.org/10.1038/nature02406.

29. **Lai R-Z, Manson JMB, Bormans AF, Draheim RR, Nguyen NT, Manson MD.** 2005. Cooperative signaling among bacterial chemoreceptors. Biochemistry (Mosc.) **44**:14298–14307. http://dx.doi.org/10.1021/bi050567y.

30. **Adler M, Erickstad M, Gutierrez E, Groisman A.** 2012. Studies of bacterial aerotaxis in a microfluidic device. Lab Chip **12**:4835–4847. http://dx.doi.org/10.1039/c2lc21006a.

31. **Tajima H, Imada K, Sakuma M, Hattori F, Nara T, Kamo N, Homma M, Kawagishi I.** 2011. Ligand specificity determined by differentially arranged common ligand-binding residues in bacterial amino acid chemoreceptors Tsr and Tar. J. Biol. Chem. **286**:42200–42210. http://dx.doi.org/10.1074/jbc.M111.221887.

32. **Lin L-N, Li J, Brandts JF, Weis RM.** 1994. The serine receptor of bacterial chemotaxis exhibits half-site saturation for serine binding. Biochemistry (Mosc.) **33**:6564–6570. http://dx.doi.org/10.1021/bi00187a025.

33. **Gardina PJ, Manson MD.** 1996. Attractant signaling by an aspartate chemoreceptor dimer with a single cytoplasmic domain. Science **274**:425–426. http://dx.doi.org/10.1126/science.274.5286.425.

34. **Gardina PJ, Bormans AF, Manson MD.** 1998. A mechanism for simultaneous sensing of aspartate and maltose by the Tar chemoreceptor of Escherichia coli. Mol. Microbiol. **29**:1147–1154. http://dx.doi.org/10.1046/j.1365-2958.1998.00964.x.

35. **Ames P, Zhou Q, Parkinson JS.** 2008. Mutational analysis of the connector segment in the HAMP domain of Tsr, the Escherichia coli serine chemoreceptor. J. Bacteriol. **190**:6676–6685. http://dx.doi.org/10.1128/JB.00750-08.

36. **Zhou Q, Ames P, Parkinson JS.** 2009. Mutational analyses of HAMP helices suggest a dynamic bundle model of input-output signalling in chemoreceptors. Mol. Microbiol. **73**:801–814. http://dx.doi.org/10.1111/j.1365-2958.2009.06819.x.

37. **Biemann HP, Koshland DE.** 1994. Aspartate receptors of Escherichia coli and Salmonella typhimurium bind ligand with negative and half-of-the-sites cooperativity. Biochemistry (Mosc.) **33**:629–634. http://dx.doi.org/10.1021/bi00169a002.

38. **Englert DL.** 2009. Microfluidic systems for investigating bacterial chemotaxis and colonization. Ph.D. dissertation. Texas A&M University, College Station, TX.

39. **Maddock JR, Shapiro L.** 1993. Polar location of the chemoreceptor complex in the Escherichia coli cell. Science **259**:1717–1723. http://dx.doi.org/10.1126/science.8456299.

40. **Block SM, Segall JE, Berg HC.** 1982. Impulse responses in bacterial chemotaxis. Cell **31**:215–226. http://dx.doi.org/10.1016/0092-8674(82)90421-4.

41. **Block SM, Segall JE, Berg HC.** 1983. Adaptation kinetics in bacterial chemotaxis. J. Bacteriol. **154**:312–323.

42. **Cluzel P, Surette M, Leibler S.** 2000. An ultrasensitive bacterial motor revealed by monitoring signaling proteins in single cells. Science **287**:1652–1655. http://dx.doi.org/10.1126/science.287.5458.1652.

43. **Adler J, Hazelbauer GL, Dahl MM.** 1973. Chemotaxis toward sugars in Escherichia coli. J. Bacteriol. **115**:824–847.

44. **Kennedy EP.** 1970. The lactose permease system of Escherichia coli, p 49–92. *In* Beckwith JR, Zipser D (ed), The lactose operon. Cold Spring Harbor Laboratory, Cold Spring Harbor, NY.

45. **Zabin I, Fowler AV.** 1970. β-Galactosidase and thiogalactoside transacetylase, p 27–47. *In* Beckwith JR, Zipser D (ed), The lactose operon. Cold Spring Harbor Laboratory, Cold Spring Harbor, NY.

46. **Boos W.** 1969. The galactose binding protein and its relationship to the beta-methylgalactoside permease from Escherichia coli. Eur. J. Biochem. **10**:66–73.

47. **Kondoh H, Ball CB, Adler J.** 1979. Identification of a methyl-accepting chemotaxis protein for the ribose and galactose chemoreceptors of Escherichia coli. Proc. Natl. Acad. Sci. U. S. A. **76**:260–264. http://dx.doi.org/10.1073/pnas.76.1.260.

48. **Etienne-Mesmin L, Chassaing B, Sauvanet P, Denizot J, Blanquet-Diot S, Darfeuille-Michaud A, Pradel N, Livrelli V.** 2011. Interactions with M cells and macrophages as key steps in the pathogenesis of enterohemorrhagic Escherichia coli infections. PLoS One **6**:e23594. http://dx.doi.org/10.1371/journal.pone.0023594.

49. **Li M, Hazelbauer GL.** 2004. Cellular stoichiometry of the components of the chemotaxis signaling complex. J. Bacteriol. **186**:3687–3694. http://dx.doi.org/10.1128/JB.186.12.3687-3694.2004.

50. **Hegde M, Englert DL, Schrock S, Cohn WB, Vogt C, Wood TK, Manson MD, Jayaraman A.** 2011. Chemotaxis to the quorum-sensing signal AI-2 requires the Tsr chemoreceptor and the periplasmic LsrB AI-2-binding protein. J. Bacteriol. **193**:768–773. http://dx.doi.org/10.1128/JB.01196-10.

51. **Hansen MC, Palmer RJ, Jr, Udsen C, White DC, Molin S.** 2001. Assessment of GFP fluorescence in cells of *Streptococcus gordonii* under conditions of low pH and low oxygen concentration. Microbiology **147**:1383–1391.